Astronomy & Astrophysics manuscript no. HBL_aa_MArev2_DJT1
November 22, 2018

Identifying TeV source candidates among *Fermi*-LAT unclassified blazars using Artificial Neural Networks

G. Chiaro[1,2], M. Meyer[3], M. Di Mauro[3], D. Salvetti[2], and G. La Mura[4] and D.J Thompson[5]

[1] Corresponding author: Graziano Chiaro, graziano.chiaro@inaf.it

[2] Institute of Space Astrophysics & Cosmic Physics, INAF, Via Bassini 15, I-20133 Milano Italy

[3] Kavli Institute for Particle Astrophysics and Cosmology, Dpt. of Physics, SLAC, Stanford University, Stanford, California 94305, USA

[4] Physics & Astronomy Dept. University of Padova Via Marzolo 8, I-35131 Padova Italy

[5] NASA Goddard Space Flight Center, Greenbelt, MD 20771 USA

November 22, 2018

ABSTRACT

Blazars and in particular the subclass of high synchrotron peaked objects are the main targets for the present generation of Imaging Atmospheric Cherenkov Telescopes (IACTs) and will remain of great importance for very high-energy γ-ray science in light of the future Cherenkov Telescope Array (CTA). **Observations by IACTs, which have small fields of view, are limited by observing conditions; therefore, it is important to select the most promising targets in order to save observation time and consequently to increase the number of detections. The aim of this paper is to search for unclassified blazars that are likely detectable with IACTs or CTA, using an artificial neural network algorithm and updated analysis of *Fermi* Large Area Telescope data.** We select 80 γ-ray sources, and for these sources we study their light curves and, for the highest-confidence candidates, potential detectability by IACTs and CTA. Follow-up observations with IACTs of our source candidates could significantly increase the current TeV source population sample and could ultimately confirm the efficiency of our algorithm to select TeV sources. It could also lead to a revision of the predicted number of sources that will be detected in the CTA extragalactic survey.

Key words. Galaxies : active, gamma rays

1. Introduction

Blazars, the most powerful Active Galactic Nuclei (AGNs), have a relativistic jet pointing toward the observer (Abdo et al. 2010; Massaro et al. 2015), showing rapid variability and high optical and radio polarization. Such objects are the most numerous class of extragalactic sources detected by TeV telescopes, the most sensitive of which are the Imaging Atmospheric Cherenkov Telescopes (IACTs) such as the existing MAGIC, H.E.S.S., and VERITAS facilities and the upcoming Cherenkov Telescope Array (CTA). **Despite their high sensitivity, however, observations by current IACTs are limited by their small fields of view, weather conditions, the need for relatively dark night skies, and by a high background that requires fairly long observations. A source with a flux of ∼1% of the Crab nebula flux requires around 50 hours of observation time. IACTs typically take data for only about 1200 hours per year (De Naurois et al. 2015). Those constraints provide a strong incentive to identify likely targets for IACT observations.**

The all-sky observations with the Large Area Telescope (LAT) on the *Fermi Gamma-ray Space Telescope (Fermi)* at GeV energies offer opportunities to find such targets. An example is the Third Catalogue of Hard Fermi-LAT Sources (3FHL: Ajello et al. 2017), which selects TeV-telescope candidates based on flux and spectral index.

An alternative approach to searching for TeV candidates is to find objects belonging to a class of sources likely to be seen at TeV energies. For extragalactic sources, this means identifying AGN that have a peak energy output at high optical frequencies. Blazar Spectral Energy Distributions (SEDs) show two broad humps in a νf_ν representation. The low-energy hump is attributed to synchrotron radiation, and the high-energy one is usually thought to be due to inverse Compton radiation (IC) (Ghisellini 2013). Based on the position of the peak of the synchrotron hump (ν^S_{peak}) in the SED, blazars are divided into three subclasses: low-synchrotron-peaked (LSP, with $\nu^S_{peak} < 10^{14}$ Hz), intermediate-synchrotron-peaked (ISP, with 10^{14} Hz $< \nu^S_{peak} < 10^{15}$ Hz) and high-synchrotron-peaked (HSP, with $\nu^S_{peak} > 10^{15}$ Hz) (Abdo et al. 2010). **In this study we refer to those three subclasses as listed in the Third Catalogue of Active Galactic Nuclei detected by the *Fermi* LAT (3LAC: Ackermann et al. 2015). Synchrotron-peak data come from the visual inspection of each LAT blazar SED by a team of *SEDders* [1] who fitted the SEDs in order to obtain the peak frequency and the classification of the source.** HSPs, primarily BL Lac objects, represent the most

[1] https://www.asdc.asi.it/

numerous class of extragalactic TeV-energy sources. The TeVCat[2] is an online, interactive catalog for very-high-energy (VHE energies, $E > 50$ GeV) γ-ray astronomy (Horan et al. 2008). The catalogue reports 211 TeV sources, where 48 of them are HSPs and only 7 are LSP/ISP flat-spectrum radio quasars (FSRQs) [3] **An example of searching out HSP candidates is the second *WISE* High Synchrotron Peak catalogue (2WHSP) (Chang et al. 2017), which is an independent list of HSP candidates based on the multi-frequency analysis of γ-ray source candidates away from the Galactic Plane. The 2WHSP catalogue resulted from a cross-match of a number of multi-wavelength surveys (in the radio, infrared, and X-ray bands) and applied selection criteria based on the radio to IR and IR to X-ray spectral slopes.**

The present search for TeV source candidates uses a two-step approach: (1) We use γ-ray variability information to search out potential HSPs among the unclassified *Fermi*-LAT sources; and (2) We analyze γ-ray spectra of these sources using more *Fermi*-LAT data than are available in published catalogues, in order to determine which of these HSP candidates are most likely to be detectable at TeV energies. The starting point is the third *Fermi*-LAT all-sky catalogue of sources detected at energies between 100 MeV and 300 GeV (3FGL: Acero et al. 2015). **The 3FGL catalogue lists 3033 γ-ray sources, of which 1745 are AGNs, mostly BL Lacs and FSRQs, and includes γ-ray source locations, energy spectra, variability information on monthly time scales, and likely associations with objects seen at other wavelengths. However in the catalogue 573 sources remain of uncertain blazar type (BCUs) and 1010 objects are unassociated with a counterpart at other wavelengths (UCSs).**

Although BCUs and UCSs often lack optical spectra and sufficient information for a rigorous classification, statistical methods (e.g., Chiaro et al. 2016; Saz Parkinson et al. 2016; Salvetti et al. 2017; Leufaucheur et al. 2017) allow likely classifications of these sources. In particular, (Salvetti et al. 2017) found 559 of the UCS sources have characteristics similar to those of AGN. These UCS_{agns} are combined with the original 573 BCUs to provide the targets for our search. We focus on the uncertain types of blazars as ones less likely to have been studied by other methods. **The Artificial Neural Network (ANN) algorithm is a common method for statistical studies of this type. We apply an optimized version of the ANN algorithm used by (Chiaro et al. 2016) to search for HSP candidates in order to select new extragalactic TeV-energy sources .**

The paper is organized as follows: in Sect. 2 we present the machine learning method used in this study; in Sect. 3 we describe the selection of HSP candidates among the uncertain 3FGL objects; and in Sect. 4 we discuss the results of a dedicated *Fermi*-LAT analysis of the sources found analyzing 104 months of data. In Sect. 5 we examine the detectability

[2] http://tevcat.uchicago.edu/

[3] The rest the sources in TeVCat are Galactic sources or of unidentified nature.

of the targets by the present generation of IACTs and CTA. In Sect. 6 we discuss the final results of this study.

2. The search method

This study is based on the two-layer-perceptron ANN technique (Gish 1990). Because of the relatively low complexity of our data, we use an optimized version of an ANN algorithm described by (Chiaro et al. 2016), with a simple structure known as Feed Forward multi-layer perceptron and in particular two-layer perceptron. In an ANN analysis, 3FGL sources with known classifications are used to train the algorithm to distinguish each source class on the basis of a parameter pattern that describes specific properties of a source. The algorithm computes a likelihood value arranged to have two possibilities: class A or class B, with a likelihood (L) assigned to each analyzed source so the likelihoods to belong to either of the two classes are related by $L_A = 1 - L_B$. In this way, the greater the value of L_A, the greater the likelihood that the source is a class A candidate.

We optimized the algorithm described in (Chiaro et al. 2016), considering three synchrotron peak subclasses as classified in the 3LAC catalogue. We used as the basic input their monthly E>100 MeV γ-ray flux values, making our predictions independent of multiwavelength data. We construct an empirical cumulative distribution function for each source: the cumulative percentage of monthly flux values less than a given flux as a function of the flux values. We include in the algorithm values corresponding to 10th, 20th, 30th, 40th, 50th, 60th, 70th, 80th, 90th, and 100th percentile of the cumulative flux distribution function for each source. While training and optimizing the algorithm, we also tested the possibility to improve the performance of the network adding the Variability Index from the 3FGL catalogue as a further parameter. Defining the importance of each ANN input parameter as the product of the mean-squared of the input variables with the sum of the weights-squared of the connection between the variable's nodes in the input layer and the hidden layer, we found the Variability Index to be, in our algorithm, an unimportant parameter. Fig. 1 shows the distribution of the Variability Index for 3FGL BL Lacs and FSRQs.

In order to optimize the training of the network to recognize HSP candidates, we considered 289 HSPs and 824 non-HSP objects classified in the 3FGL catalogue. Maintaining the same ratio as in the 3FGL catalogue, that is, one third HSPs and two thirds non-HSP sources, we randomly mixed the sample and used one third for training the algorithm, one third for optimization and remaining for testing respectively. Applying our algorithm to the training sample produces a likelihood distribution with a concentration for non-HSP sources at low L_{HSP} and a relatively flat distribution for HSPs. Fig. 2 shows that the likelihood distribution can be used in our study to reject non-HSP-type blazars. **Assessing**

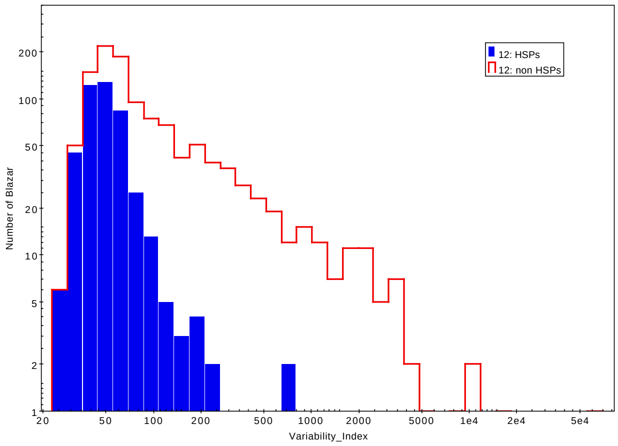

Fig. 1. Variability Index distribution for 3FGL HSPs (blue filled columns) and non HSPs (red steps). The histograms show a significant overlap that confirms the Variability Index as an unimportant parameter for our purpose.

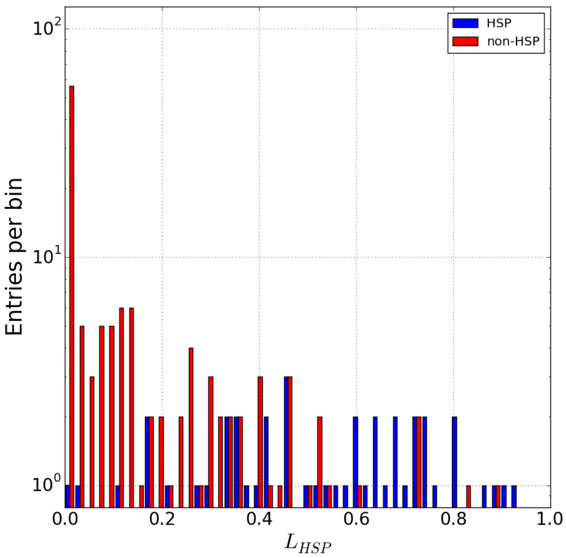

Fig. 2. Likelihood distribution of known HSP and non-HSP sources with our ANN algorithm.

the completeness of the sample and the fraction of spurious sources labelled as HSP-like or non HSP-like candidates we define two classification thresholds. The former is based on the optimization of the positive association rate (precision). It is defined as the fraction of true positives with respect to the objects classified as positive, of $\sim 90\%$. The latter based on the sensitivity, defined as the fraction of objects of a specific class correctly classified as such, referenced to the defined threshold, $L_{HSP} > 0.8$

3. Identifying HSP candidates

We applied the optimized ANN algorithm to the 573 BCUs and the 559 UCS$_{agn}$ of our sample. The likelihood distribution of both groups of sources is shown in Fig. 3. The resulting likelihood distributions show, as we expected, a peak at $L_{HSP} = 0.0$ due to the

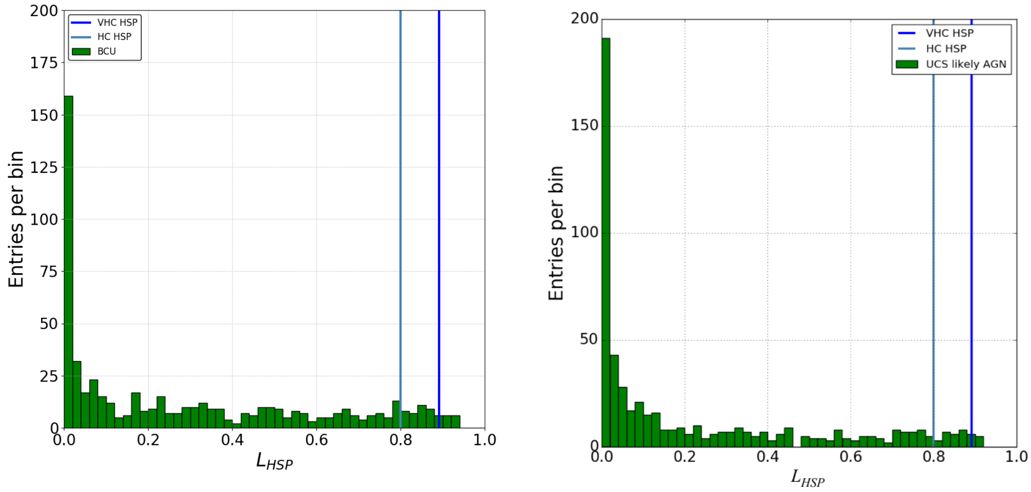

Fig. 3. Distribution of the ANN likelihood to be HSP candidates of 3FGL BCUs (left) and UCS$_{agn}$ (right). Vertical blue and steel blue lines indicate the classification thresholds of our ANN algorithm to identify sources with a $L_{HSP} > 0.8$ and HC candidates with $L_{HSP} > 0.891$.

non-HSP populations (ISP and LSP), which are much more numerous than HSPs. **Requiring the $L_{HSP} > 0.8$ value, we identified 48 BCU and 32 UCS$_{agn}$ as HSP candidates. In order to have the cleanest candidates we define an even narrower threshold value $L_{HSP} > 0.891$ (true positive ratio $\sim 90\%$) that limits the non-contamination area in Fig. 3. Applying this further threshold, we identified 11 BCUs and 5 UCS$_{agn}$ named High Confidence (HC) HSP candidates. In Table 1 and Table 2 the full lists of candidates are shown, where the HC sources are on the top of the list.**

In Figure 4 we show the properties of the HC candidates (black dots) compared to those of the 3FGL blazar subclasses HSP (blue), LSP (red), and ISP (green) in a 3D plot: γ-ray flux, Variability Index, and spectral index. All the candidates lie in a clean HSP area of the plot and far from the LSPs (red). We also compare the HSP candidates with the 2WHSP catalogue (Chang et al. 2017), and 36 sources in Table 1 and Table 2 are also in the 2WHSP catalogue. **Those results reinforce the ability of the algorithm to select consistent candidates.**

4. Fermi-LAT Spectral Analysis

We performed an analysis of *Fermi*-LAT data analyzing 104 months of Pass 8 data, from 2008 August 4 to 2017 April 4, selecting γ-ray events in the energy range $E = [0.1, 1000]$ GeV, passing standard data quality selection criteria, in order to find the γ-ray properties of our HSP candidates. We considered events belonging to the Pass 8 `SOURCE` event class and used the corresponding instrument response functions `P8R2_SOURCE_V6`, since we were interested in

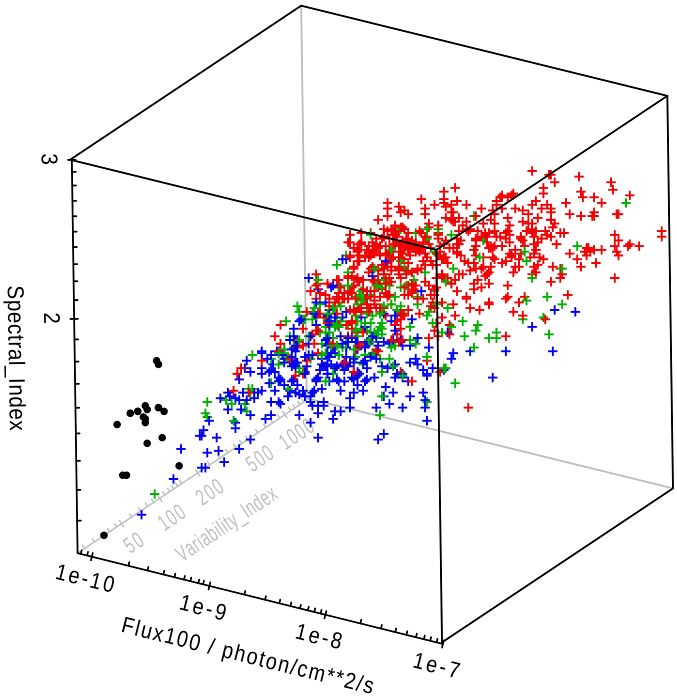

Fig. 4. HC candidate (black dots) properties compared to those of the 3FGL blazar subclasses HSP (blue), IBL (green), and LBL (red).

point source detection. We used the interstellar emission model (IEM) released with Pass 8 data (Acero et al. 2016) (i.e., `gll_iem_v06.fits`). This is the model routinely used in Pass 8 analyses. We also included the standard template for the isotropic emission (`iso_P8R2_SOURCE_V6_v06.txt`) [4].

We developed an analysis pipeline using `FermiPy`, a Python package that automates analyses with the *Fermi* Science Tools (Wood M. 2017)[5]. `FermiPy` includes tools that can 1) generate simulations of the γ-ray sky, 2) detect point sources, and 3) calculate the characteristics of their SEDs. For more details on `FermiPy` we refer to the Appendices of (Ajello et al. 2017). **The likelihood analysis works on a square region of interest (ROI). We used a** $16^{\circ} \times 16^{\circ}$ **ROI centered on the sources of our sample. We analyzed each ROI separately. In each ROI, we binned the data with a pixel size of** 0.08° **and 8 energy bins per decade. Our model includes the IEM, isotropic template and sources from the preliminary 8-year list[6]. We allowed the normalization and slopes of the IEM and isotropic templates to vary.** We first relocalized the source of interest, and then we searched for new point sources with Test Statistic $TS > 25$, defined as twice the difference between the log-likelihood for the null hypothesis (no source) and the hypothesis of a source at the location. After this first step we calculated the SED

[4] For descriptions of these templates, see `http://fermi.gsfc.nasa.gov/ssc/data/access/lat/BackgroundModels.html`.
[5] See `http://fermipy.readthedocs.io/en/latest/`.
[6] `https://fermi.gsfc.nasa.gov/ssc/data/access/lat/fl8y/gll_psc_8year_v5.fit`

of the source and we computed its lightcurve in order to determine whether the source is variable. The variability was estimated for each source by calculating the Test Statistic for variability (TS_{VAR}), defined as twice the difference between the log-likelihood for the null hypothesis (constant flux in time) and the hypothesis of a variable flux.

In Table 1 and Table 2 we report the spectral index, TS_{VAR} and TS for detection of the HSP candidates. The spectral index parameter, if less than 2, can be a relevant indicator for an IC peak at TeV energies and therefore quite useful in selecting IACT or CTA candidates. The mean and rms of the spectral indexes of HSPs are 1.87 ± 0.20 while for LSPs and ISPs these are 2.21 ± 0.18, 2.07 ± 0.20 respectively.

5. TeV candidates

In this section, we compare the extrapolated fluxes of these sources against the sensitivity of present IACTs and the future CTA. We use the *Fermi*-LAT spectral shapes obtained in the previous section and focus further analysis on the HC candidates. In order to evaluate whether the HC HSP candidates can realistically be observed with IACTs or CTA, we must take into account the interaction of γ-rays with photons of the extragalactic background light (EBL). The relevant part of the EBL spans the wavelength regime from ultraviolet to far-infrared wavelengths and mainly consists of the integrated starlight emitted over the history of the Universe and starlight absorbed and re-emitted by dust in galaxies (Hauser et al. 2001; Kashlinsky et al. 2005). During the propagation of γ rays through the EBL, the electron-positron pairs produced via $\gamma\gamma \rightarrow e^{+}e^{-}$ leads to an attenuation of the initial γ-ray flux (Nikisov et al. 1962; Gould et al. 1967; Dwek et al. 2013). To properly evaluate the absorption effect of the EBL it is necessary to know the redshift of the analyzed γ-ray source. Since the redshifts of the selected HC HSP candidates are unknown, we assume redshifts between $z = 0$ and $z = 0.5$, which are typical values of observed γ-ray BL Lacs. **We used these z values while recognizing that blazar redshift range is a very open and long standing debate. Some authors argue that the BL Lacs without a redshift are likely much more distant than those with a measured one (e.g., Padovani et al. 2012), so it could be possible that some objects fall beyond the 0-0.5 redshift range.**

Using the EBL model of Dominguez et al. (2011), we extrapolate the best-fit spectra obtained with the *Fermi* analysis in Sec. 4 up to 10 TeV with the assumed redshift values. The results are shown in Fig. 5 and Fig. 6 where we compare the extrapolated fluxes with the CTA sensitivity for 50 hours (5 hours) of observations as a solid (dashed) grey line. Above a declination of 0° we use the sensitivity of the northern array and otherwise that of the southern array[7]. The CTA sensitivity for 5 hours of observation is similar to that of currently operating IACTs for

[7] The sensitivity curves of the northern and southern array are available at `www.cta-observatory.org`

50 hours of observation, although the current IACTs have typically a higher threshold energy of $\gtrsim 80$ GeV. For a redshift of $z = 0.5$ most of the considered sources should still be detectable by currently operating IACTs and appear to be good candidates for detection with CTA. In Table 1 and Table 2 we also highlight the "observability" with current IACTs for the objects that rise above 30° from the local horizon from the observing sites, which corresponds to the zenith angle cut of values smaller than 60° commonly adopted for these IACTs. In Table 3, we report the maximum redshift values of the TeV candidates so that the sources are still detectable at $5\,\sigma$ for 5- and 50-hour CTA observations. If no value is given, the source will not be significantly detected with the assumed observation time at any redshift.

6. Conclusion

Motivated by wishing to expand the sample of TeV sources, we have developed a search method based on machine learning applied to variability parameters of *Fermi*-LAT blazar-like sources without firm identifications combined with new analysis of the LAT data for these sources. Follow-up work will necessitate additional multiwavelength studies, including finding redshifts for most of the candidates and targeted observation by IACTs. We also recognize that this search is necessarily incomplete because of the difficulty to distinguish the blazar subclasses by the γ-ray properties only. As already pointed out by Ackermann et al. (2015), the γ-ray sources with unknown properties are generally fainter than the well-defined classes. **The fainter sources offer less of the variability information needed for the machine learning method, and so there may be HSP blazars among the sample 3FGL sources computed in the first step of our method. The level of incompleteness is difficult to quantify due to the very similar values of the synchrotron peaks of the three blazar subclasses. Nevertheless, the HC HSP candidates, also thanks to the analysis of *Fermi*-LAT data, are convincing as TeV candidates and could be promising targets for CTA observations for population studies.**

7. Acknowledgments

The *Fermi* LAT Collaboration acknowledges generous ongoing support from a number of agencies and institutes that have supported both the development and the operation of the LAT as well as scientific data analysis. These include the National Aeronautics and Space Administration and the Department of Energy in the United States, the Commissariat à l'Energie Atomique and the Centre National de la Recherche Scientifique / Institut National de Physique Nucléaire et de Physique des Particules in France, the Agenzia Spaziale Italiana and the Istituto Nazionale di Fisica Nucleare in Italy, the Ministry of Education, Culture, Sports, Science and Technology (MEXT), High Energy Accelerator Research Organization (KEK) and Japan Aerospace Exploration Agency (JAXA) in Japan, and the K. A. Wallenberg Foundation, the Swedish Research Council and the Swedish National Space Board in Sweden.

Additional support for science analysis during the operations phase is gratefully acknowledged from the Istituto Nazionale di Astrofisica in Italy and the Centre National d'Études Spatiales in France. This work performed in part under DOE Contract DE-AC02-76SF00515.

MDM acknowledges support by the NASA *Fermi* Guest Investigator Program 2014 through the *Fermi* multi-year Large Program No. 81303 (P.I. E. Charles) and by the NASA *Fermi* Guest Investigator Program 2016 through the *Fermi* one-year Program No. 91245 (P.I. M. Di Mauro).

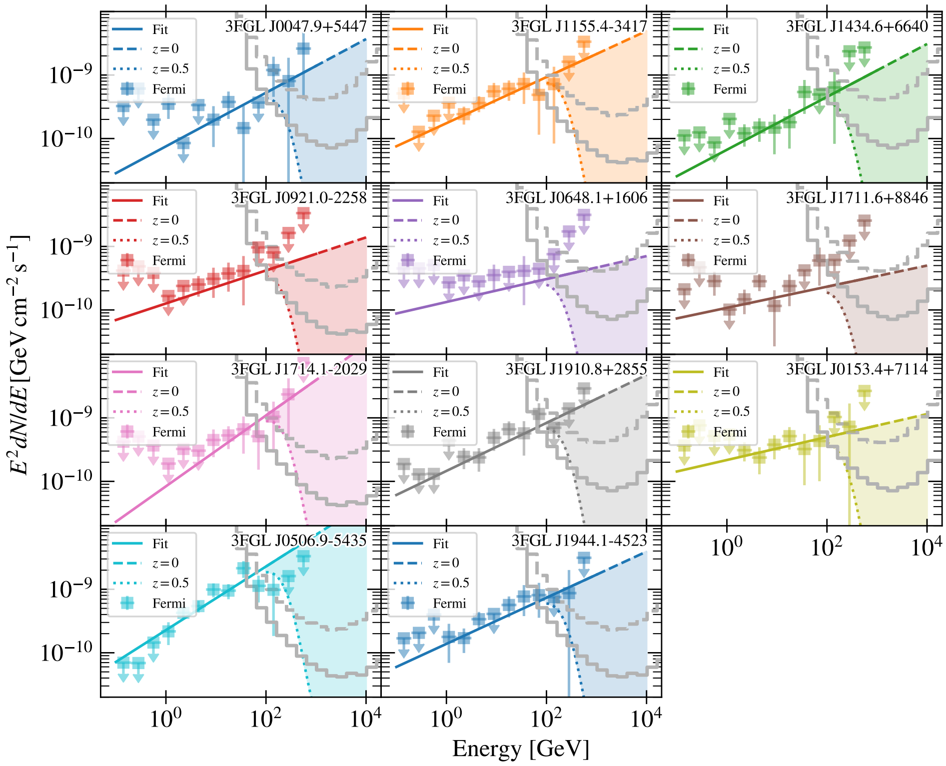

Fig. 5. SEDs of the HC BCU sources as TeV candidates.The dashed (dotted) line denotes the extrapolation of the best-fit spectra up to 10 TeV for a redshift of $z = 0$ ($z = 0.5$) The shaded region indicates the possible source flux for redshifts between $0 < z \leq 0.5$. The CTA sensitivity for 5 (50) hours of observation is shown as a grey solid (dashed) line.

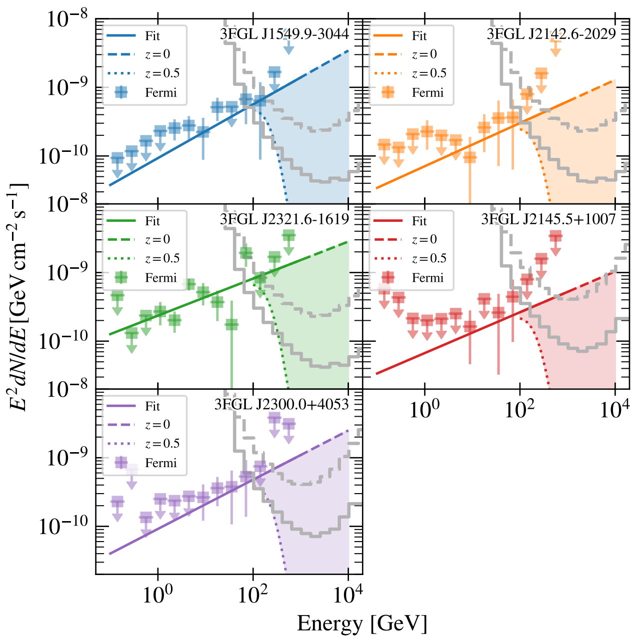

Fig. 6. SEDs of the HC UCS sources as TeV candidates.The dashed (dotted) line denotes the extrapolation of the best-fit spectra up to 10 TeV for a redshift of $z = 0$ ($z = 0.5$) The shaded region indicates the possible source flux for redshifts between $0 < z \leq 0.5$. The CTA sensitivity for 5 (50) hours of observation is shown as a grey solid (dashed) line.

Table 1. Full list of BCU HSP candidates. Columns: (1) 3FGL name; (2) Association with known source; (3) Included in 2WHSP; (4) Detection TS 0.1– 300 GeV; (5) Spectral Index; (6) Variability TS_{VAR}; (7) HSP Likelihood; (8), (9), (10) observability at IACT sites. At the top of the list are the HC sources ($L > 0.89$).

3FGL name	Association	2WHSP	TS	Sp.Index	TS_{VAR}	L_{HSP}	HESS	VERITAS	MAGIC
3FGL J0047.9+5447	1RXS J004754.5+544758		56.7	1.5	11.7	0.92		◇	◇
3FGL J1155.4-3417	NVSS J115520-341718	◇	147.3	1.6	16.2	0.92	◇		
3FGL J1434.6+6640	1RXS J143442.0+664031		73.9	1.5	16.7	0.92		◇	◇
3FGL J0921.0-2258	NVSS J092057-225721	◇	62.5	1.7	10.5	0.91	◇	◇	◇
3FGL J0648.1+1606	1RXS J064814.1+160708		40.1	1.8	13.9	0.9	◇	◇	◇
3FGL J1711.6+8846	1RXS J171643.8+884414	◇	44.3	1.8	12.4	0.9		◇	◇
3FGL J1714.1-2029	1RXS J171405.2-202747	◇	73.8	1.4	18.1	0.9	◇	◇	◇
3FGL J1910.8+2855	1RXS J191053.2+285622		102.2	1.6	15.1	0.9	◇	◇	◇
3FGL J0153.4+7114	TXS 0149+710		80.8	1.8	19.7	0.89	◇	◇	
3FGL J0506.9-5435	1ES 0505-546	◇	455.4	1.4	29.8	0.89	◇		
3FGL J1944.1-4523	1RXS J194422.6-452326	◇	100.6	1.6	11.1	0.89	◇		
3FGL J0742.4-8133c	SUMSS J074220-813139		32.2	2.0	11.8	0.88			
3FGL J0043.7-1117	1RXS J004349.3-111612	◇	69.4	1.9	12.5	0.88			
3FGL J1824.4+4310	1RXS J182418.7+430954	◇	80.9	1.8	19.7	0.88			
3FGL J0528.3+1815	1RXS J052829.6+181657		35.6	1.6	14.6	0.87			
3FGL J0646.4-5452	PMN J0646-5451		190.3	1.4	17.3	0.87			
3FGL J0040.3+4049	B3 0037+405	◇	75.9	1.9	12.0	0.87			
3FGL J1959.8-4725	SUMSS J195945-472519	◇	923.7	1.5	94.3	0.87			
3FGL J2108.6-8619	1RXS J210959.5-861853	◇	91.0	1.6	10.7	0.87			
3FGL J0039.0-2218	PMN J0039-2220	◇	89.3	1.6	11.6	0.86			
3FGL J0305.2-1607	PKS 0302-16		147.6	1.6	22.9	0.86			
3FGL J1040.8+1342	1RXS J104057.7+134216	◇	69.1	1.7	11.0	0.86			
3FGL J2312.9-6923	SUMSS J231347-692332	◇	35.3	1.7	16.1	0.86			
3FGL J0515.5-0123	NVSS J051536-012427		45.6	1.7	11.7	0.85			
3FGL J0620.4+2644	RX J0620.6+2644	◇	92.0	1.5	15.1	0.85			
3FGL J0640.0-1252	TXS 0637-128	◇	174.1	1.5	14.4	0.85			
3FGL J0733.5+5153	NVSS J073326+515355	◇	104.3	1.6	11.1	0.85			
3FGL J1141.2+6805	1RXS J114118.3+680433		140.0	1.6	23.3	0.85			
3FGL J1203.5-3925	PMN J1203-3926	◇	103.2	1.6	18.5	0.85			
3FGL J1939.6-4925	SUMSS J193946-492539		64.5	1.8	15.9	0.85			
3FGL J2316.8-5209	SUMSS J231701-521003		37.3	1.7	15.1	0.85			
3FGL J0132.5-0802	PKS 0130-083		71.9	1.87	12.4	0.8			
3FGL J0342.6-3006	PKS 0340-302		43.1	1.96	13.3	0.8			
3FGL J1446.8-1831	NVSS J144644-182922	◇	27.9	1.7	8.6	0.84			
3FGL J1855.1-6008	PMN J1854-6009		21.3	1.8	6.7	0.84			
3FGL J0043.5-0444	1RXS J004333.7-044257	◇	75.9	1.9	11.9	0.83			
3FGL J0746.9+8511	NVSS J074715+851208	◇	118.9	1.6	18.3	0.83			
3FGL J0650.5+2055	1RXS J065033.9+205603		206.2	1.7	20.0	0.82			
3FGL J1319.6+7759	NVSS J131921+775823		182.6	1.9	25.1	0.82			
3FGL J1908.8-0130	NVSS J190836-012642		306.4	2.1	35.5	0.82			
3FGL J2347.9+5436	NVSS J234753+543627		163.0	1.7	21.7	0.82			
3FGL J0204.2+2420	B2 0201+24		27.6	1.7	12.	0.81			
3FGL J0439.6-3159	1RXS J043931.4-320045	◇	119.8	1.7	24.9	0.81			
3FGL J1547.1-2801	1RXS J154711.8-280222		96.7	1.7	16.7	0.81			
3FGL J1612.4-3100	NVSS J161219-305937	◇	494.9	1.8	116.1	0.81			
3FGL J0030.2-1646	1RXS J003019.6-164723	◇	168.7	1.6	30.1	0.80			
3FGL J1158.9+0818	RX J1158.8+0819	◇	51.4	1.8	11.8	0.80			
3FGL J1841.2+2910	MG3 J184126+2910	◇	195.9	1.7	22.8	0.80			

Table 2. Full list of UCS$_{agn}$ HSP candidates. Columns: (1) 3FGL name; (2) Included in 2WHSP; (3) Detection TS 0.1– 300 GeV; (4) Spectral Index; (5) Variability TS_{VAR}; (6) HSP Likelihood; (7), (8), (9) observability at IACT sites. At the top of the list are the HC sources (L> 0.89).

3FGL name	2WHSP	TS	Sp.Index	TS_{VAR}	L_{HSP}	HESS	VERITAS	MAGIC	
3FGL J1549.9-3044	◇	64.2	1.6	10.1	0.91	◇		◇	
◇3FGL J2142.6-2029		36.0	1.6	8.1	0.91	◇	◇	◇	
◇3FGL J2321.6-1619		34.1	1.7	45.1	0.91	◇	◇	◇	
◇3FGL J2145.5+1007		52.5	1.7	19.9	0.90		◇	◇	◇
◇3FGL J2300.0+4053	◇	174.5	1.6	6.9	0.90	◇	◇	◇	
3FGL J1155.3-1112		52.4	1.5	11.3	0.89				
3FGL J2224.4+0351		29.5	1.9	9.5	0.89				
3FGL J1525.8-0834	◇	59.5	1.9	23.2	0.89				
3FGL J1619.1+7538		107.1	1.8	14.9	0.88				
3FGL J0251.1-1829		104.2	1.5	10.2	0.88				
3FGL J0020.9+0323		60.6	2.0	22.5	0.88				
3FGL J0813.5-0356		57.0	1.7	13.1	0.88				
3FGL J1234.7-0437		51.5	2.0	29.7	0.87				
3FGL J1922.2+2313		80.8	2.2	22.6	0.87				
3FGL J2043.6+0001		48.4	2.0	24.4	0.87				
3FGL J0312.7-2222		177.1	1.8	18.2	0.87				
3FGL J1513.3-3719	◇	54.7	1.9	18.0	0.87				
3FGL J0524.5-6937		94.1	2.0	18.3	0.86				
3FGL J1225.4-3448		22.2	1.7	7.0	0.86				
3FGL J1222.7+7952		43.8	2.1	14.7	0.86				
3FGL J2309.0+5428	◇	77.0	1.7	17.6	0.85				
3FGL J2015.3-1431	◇	17.4	1.8	14.6	0.85				
3FGL J2053.9+2922		359.6	1.7	43.9	0.85				
3FGL J0234.2-0629		90.7	2.0	20.7	0.84				
3FGL J1545.0-6641		150.1	1.5	11.8	0.84				
3FGL J0731.8-3010		37.0	1.9	12.9	0.84				
3FGL J0952.8+0711		50.9	1.9	14.1	0.84				
3FGL J0527.3+6647		51.8	1.9	14.7	0.83				
3FGL J1528.1-2904		26.2	1.8	11.7	0.83				
3FGL J0049.0+4224	◇	36.9	1.8	16.5	0.82				
3FGL J1057.6-4051	◇	40.2	1.71	15.5	0.82				
3FGL J0928.3-5255		98.7	2.09	26.6	0.80				

Table 3. Maximum redshift values so that the BCU HC_{TeV} and UCS_{agn} HC_{TeV} are still detectable at $5\,\sigma$ in a 5 (50) hours of CTA (current IACT) observation. If no value is given, the source will not be significantly detected with the assumed observation time.

BCU HC_{TeV} candidates		
3FGL name	$z_{\max}$ ($T_{obs} = 5$ hours)	$z_{\max}$ ($T_{obs} = 50$ hours)
3FGL J0047.9+5447	0.15	> 0.50
3FGL J1155.4-3417	0.40	> 0.50
3FGL J1434.6+6640	0.12	> 0.50
3FGL J0921.0-2258	0.11	> 0.50
3FGL J0648.1+1606	0.01	0.29
3FGL J1711.6+8846	—	0.19
3FGL J1714.1-2029	> 0.50	> 0.50
3FGL J1910.8+2855	0.25	> 0.50
3FGL J0153.4+7114	0.07	> 0.50
3FGL J0506.9-5435	> 0.50	> 0.50
3FGL J1944.1-4523	0.29	> 0.50
UCS_{agn} HC_{TeV} candidates		
3FGL J1549.9-3044	0.21	> 0.50
3FGL J2142.6-2029	0.08	0.42
3FGL J2321.6-1619	0.31	> 0.50
3FGL J2145.5+1007	0.02	0.26
3FGL J2300.0+4053	0.12	> 0.50

References

Abdo A.A. , Ackermann M., Agudo I. et al., 2010, ApJ, 716,30

Acero F., Ackermann, M., Ajello M. et al. , 2015, ApJS, 218, 23

Acero F., Ackermann, M., Ajello M. et al. , 2016, ApJS 223, 26

Ackermann, M., Ajello, M., Atwood W.B. et al., 2015, ApJ 810, 14, 34

Aharonian A. , Akhperjanian A., Bazer-Bachi A. et al., 1993, ExA, 2, 331

Ajello M., Atwood W. B.,Baldini L. et al., 2017, ApJS, 232, 18

Ajello, M. , Baldini L., Ballet J. et al., 2017, ArXiv: 1705.00009

Alvarez Crespo N., Masetti N., Ricci F. et al., 2016 AJ, 151, 32

Ambrogi L. , Celli S., Aharonian A. et at., 2018, APh, 69 , 79

Angioni R. , Grandi P., Torresi E. et al., 2017, APh, 92,42

Arsioli B., Chang Y., 2017, A&A, 598, 134

Arsioli B., Giommi P.,Fragon B. et al, 2015, A&A, 579, 34

Atwood W. B. , Abdo A. A., Ackermann M. et al., 2009, ApJ, 697, 1071

Bishop C.M., Neural Network for Pattern Recognition, 1995

Carosi A. , 2015, Proceeding of the 34th International Cosmic Ray Conference, p. 5

Chang Y.L. , Arsioli B., Giommi P. et al. , 2017, A&A , 598, 17

Chiaro G. , D.Salvetti, G. La Mura et al., 2016 MNRAS 462.3.3180C

Costamante L. , 2002, A&A, 384, 56

De Naurois M., Mazin D. , 2015, Comptes rendus - Physique, 16, 610

De Naurois M, Rolland L. , 2009, Aph, 32, 331

Doert M. , Errando M., 2014, ApJ, 782, 41

Dwek E. , Krennrich F. , 2013, APh, 43,112

Dominguez A. , Primack J. R.; Rosario D. J. et al.,2011, MNRAS ,410,2556

Ghisellini G., 2013, EPJ Web of Conference, Vol. 61, id.05001.

Gish H., 1990, Proceeding on Acoustic Speech and Signal Processing, p. 1361

Gould R., Schreder G.,1967, Ph Rv, 155, 1408

Hassan T., Dominguez A., Leufaucher J. et al, 2013, arxiv 1708.0774

Hauser M., DweK E. , 2001,ARAA, 2001,39,249
Hillas A.M. , Akerlof, C. W., Biller, S. D et al., 1998, ApJ, 503, 744
Horan D., Wakeley S., 2008, AAS, HEAD meeting 10, id.41.06
Hoecker, A., Speckmayer, P., Stelzer, J., et al. ,2007, ArXiv Physics 0703039
Kolmogorov A., 1933, G. Ist. Ital. Attuariale 4, 83
Kashlinsky A. et al.,2005, 409,361
Leufaucheur J., Pita S. 2007, A&A, 602,86
Lott B. , Escande, L., Larsson, S et al., 2012, A&A, 544, A6
Massaro F., Paggi A. , Errando M. et al., 2013, ApJS, 207,16
Massaro F. , Landoni R. D'Abrusco D. et al.,2015,A&A, 24, 2
Nikisov A., 1962, Sov.Phys., 14,393
Padovani P., Giommi P., Rau A., 2012, MNRAS, 422, 48
Pita S. , 2017, AIPC, 1792,25
Richard M. P., and Lippman R. P., 1991, Neural Computation, 3, 461
Rieger F.M. , Wilhelmi, E., Aharonian A. et al, 2013, FrPhy, 8, 714
Rumelhart, D. E., Hinton, G. E., Williams, R. J. 1986, Nature
Saz Parkinson P., Xu H., Yu P. et al, (2016), ApJ, 820,2
Salvetti D. Chiaro G. , La Mura G. et al., 2017, MNRAS, 470, 1291
Wilks S.S., 1938, AMS, 9, 60
Wood M., Caputo R., Charles E. et al. 2017, ArXiv: 1707.09551

List of Objects